Supplemental Material for "Electron-Phonon Scattering in the Presence of Soft Modes and Electron Mobility in $SrTiO_3$ Perovskite from First Principles"

Jin-Jian Zhou,[1] Olle Hellman,[1,2] and Marco Bernardi[1,*]

[1]*Department of Applied Physics and Materials Science, California Institute of Technology, Pasadena, California 91125, USA*

[2]*Department of Physics, Boston College, Chestnut Hill, Massachusetts 02467, USA*

Correction to the long-range interatomic force constants in polar materials

The temperature dependent effective potential (TDEP) method computes phonon dispersions by assuming that the interatomic force constants (IFCs) are negligible for inter-atomic distances larger than the supercell size. However, for a polar material with non-vanishing Born effective charges, the interactions between dipoles created by atomic displacements decay as $1/d^3$, where d is the inter-atomic distance. Therefore, the IFCs in polar materials contain a long-range contribution due to the dipole-dipole interactions [1], to include which a correction is required to avoid using unrealistically large supercells.

We propose a new method to treat the long-range dipole-dipole interactions. We separate the IFCs into two parts − the long-range contribution $\mathbf{\Phi}^L$ due to the dipole-dipole interactions and the remainder $\mathbf{\Phi}^S$, which is short-ranged and negligible outside the supercell. The $\mathbf{\Phi}^L$ are cumulative force constants that include the interactions between dipoles located both inside the supercell and in all of its images due to the periodic boundary conditions [2, 3]. We evaluate $\mathbf{\Phi}^L$ using Born effective charges and the dielectric tensor from DFPT (the derivation will be detailed elsewhere):

$$\Phi_{ij}^{L,\alpha\beta} = \frac{4\pi}{N\Omega} \sum_{\boldsymbol{K}\neq\mathbf{0}} \frac{(K_\mu Z_i^{\mu\alpha})(K_\nu Z_j^{\nu\beta}) e^{i\boldsymbol{K}\cdot(\boldsymbol{r}_i-\boldsymbol{r}_j)}}{(K_\mu \cdot \boldsymbol{\epsilon}^{\mu\nu} \cdot K_\nu)} e^{\frac{-K_\mu\cdot\boldsymbol{\epsilon}^{\mu\nu}\cdot K_\nu}{4\Lambda^2}} \tag{1}$$

where $\boldsymbol{\epsilon}$ is the dielectric tensor, Λ is the convergence parameter in the Ewald summation [4], $\boldsymbol{K}$ are reciprocal lattice vectors of a supercell consisting of N unit cells with volume Ω, $\boldsymbol{Z}_i$ are Born effective charges, and $\boldsymbol{r}_i$ is the position of atom i within the supercell; α, β, μ and ν are Cartesian directions, and a summation over repeated indices is implied.

The contribution to the force on atom i due to the long-range dipole-dipole interactions is computed as $\boldsymbol{F}_i^L = -\sum_j \mathbf{\Phi}_{ij}^L \boldsymbol{u}_j$, where $\boldsymbol{u}_j$ is the displacement of atom j. By subtracting $\boldsymbol{F}_i^L$ from the Hellmann-Feynman forces computed in the DFT supercell calculations, we obtain forces $\boldsymbol{F}_i^S$ associated with the short-range part of the IFCs, $\boldsymbol{F}_i^S = -\sum_j \mathbf{\Phi}_{ij}^S \boldsymbol{u}_j$. Since the $\mathbf{\Phi}_{ij}^S$ are negligible beyond the supercell, they can be computed from the displacements $\boldsymbol{u}_i$ and forces $\boldsymbol{F}_i^S$ using a standard supercell method [2] or the typical TDEP procedure [5]. The dynamical matrices corresponding to the short- and long-range IFC contributions are then combined and diagonalized to obtain phonon energies and eigenvectors.

The long-range contribution to the dynamical matrix at wavevector $\boldsymbol{q}$ is computed as

(omitting the mass factor)

$$D^{L,\alpha\beta}_{\kappa\kappa'}(\boldsymbol{q}) = \frac{4\pi}{\Omega}\sum_{\boldsymbol{G}\neq-\boldsymbol{q}}\frac{[(q+G)_\mu Z^{\mu\alpha}_\kappa][(q+G)_\nu Z^{\nu\beta}_{\kappa'}]e^{i(\boldsymbol{q}+\boldsymbol{G})\cdot(\boldsymbol{\tau}_\kappa-\boldsymbol{\tau}_{\kappa'})}}{(q+G)_\mu\cdot\boldsymbol{\epsilon}^{\mu\nu}\cdot(q+G)_\nu}e^{\frac{-(q+G)_\mu\cdot\boldsymbol{\epsilon}^{\mu\nu}\cdot(q+G)_\nu}{4\Lambda^2}}$$
$$-\delta_{\kappa\kappa'}\frac{4\pi}{\Omega}\sum_{\kappa''}\sum_{\boldsymbol{G}\neq\boldsymbol{0}}\frac{(G_\mu Z^{\mu\alpha}_\kappa)(G_\nu Z^{\nu\beta}_{\kappa''})e^{i\boldsymbol{G}\cdot(\boldsymbol{\tau}_\kappa-\boldsymbol{\tau}_{\kappa''})}}{G_\mu\cdot\boldsymbol{\epsilon}^{\mu\nu}\cdot G_\nu}e^{\frac{-G_\mu\cdot\boldsymbol{\epsilon}^{\mu\nu}\cdot G_\nu}{4\Lambda^2}}, \tag{2}$$

where $\boldsymbol{G}$ are unit cell reciprocal lattice vectors and $\boldsymbol{\tau}_\kappa$ is the position of atom κ within the unit cell. Eq. 2 is derived from the long-range contribution to the IFCs given in Eq. 1 by creating a fictitious supercell that has the wavevector $\boldsymbol{q}$ as one of its reciprocal lattice vectors. The second term in Eq. 2 is introduced to enforce the acoustic sum rule.

We summarize our 4-step approach for computing phonon dispersions in polar materials:

1. Build supercells with different atomic displacements and perform DFT calculations on the supercells to collect the atomic displacements $\boldsymbol{u}_i$ and forces $\boldsymbol{F}_i$.

2. Evaluate (using Eq. 1) the long-range contribution to the forces, $\boldsymbol{F}^L_i$ and then obtain the short-range contribution to the forces, $\boldsymbol{F}^S_i = \boldsymbol{F}_i - \boldsymbol{F}^L_i$.

3. Compute the short-range IFCs, $\boldsymbol{\Phi}^S$, from $\boldsymbol{u}_i$ and $\boldsymbol{F}^S_i$ using a standard supercell approach or the typical TDEP procedure.

4. Compute the dynamical matrix at wavevector $\boldsymbol{q}$ by combining the short- and long-range contributions, $D(\boldsymbol{q}) = D^L(\boldsymbol{q}) + D^S(\boldsymbol{q})$, where $D^L(\boldsymbol{q})$ is computed using Eq. 2 and $D^S(\boldsymbol{q})$ is obtained from $\boldsymbol{\Phi}^S$ via Fourier transformation.

Bandstructure and effective masses of cubic $SrTiO_3$

Figure S1 below shows the electronic bandstructure for the three lowest conduction bands of cubic $SrTiO_3$. The bandstructure for energies close to the conduction band minimum (CBM), which are most relevant for charge transport calculations, is shown in the inset. The energy splitting at Γ is due to the spin-orbit coupling. Table S1 gives the effective masses along different high-symmetry directions and the spin-orbit splitting ΔE_{SO}. These quantities are computed in our work within the generalized gradient approximation [6] of DFT. Results from HSE hybrid functional calculations from Ref. [7] are also given for comparison.

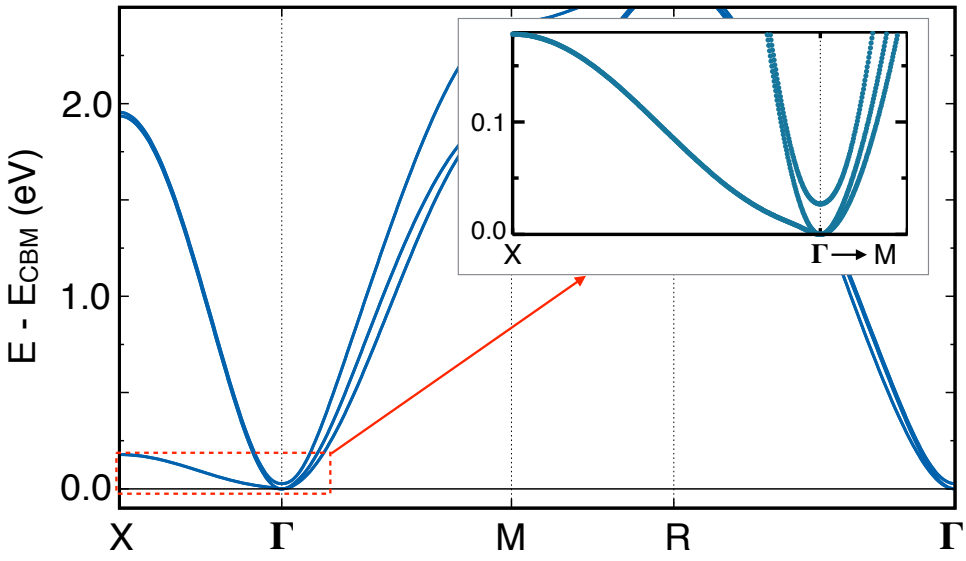

FIG. S1. Computed bandstructure of cubic $SrTiO_3$ near the conduction band minimum (CBM). The zero of the energy axis is the CBM. The inset focuses on the small energy range near the CBM of relevance for charge transport. Note that electrons at Γ cannot be scattered to R by absorbing an AFD soft phonon due to the large energy difference between the electronic states at Γ and R.

TABLE S1. Computed electron effective masses (in units of the electron mass) along the Γ−X and Γ−M directions in cubic $SrTiO_3$. The spin-orbit splitting at Γ, ΔE_{SO}, is also given. The first, second and third lowest conduction bands are denoted in the table as CB-1, CB-2 and CB-3, respectively. The HSE hybrid functional results from Ref. [7] are also given for comparison.

	Γ−X			Γ−M			ΔE_{SO}(meV)
	CB-1	CB-2	CB-3	CB-1	CB-2	CB-3	
This work	1.16	0.39	0.54	0.75	0.47	0.56	27
HSE	0.99	0.39	0.55	0.74	0.46	0.56	28

Comparison of electron mobilities computed using different approaches

Figure S2(a) compares the electron mobility obtained using the relaxation time approximation (RTA) and the iterative solution of the Boltzmann transport equation (BTE). The mobilities from the RTA and the iterative BTE exhibit a similar temperature dependence, though the temperature dependence in the iterative BTE result ($T^{-3.12}$) is in better agree-

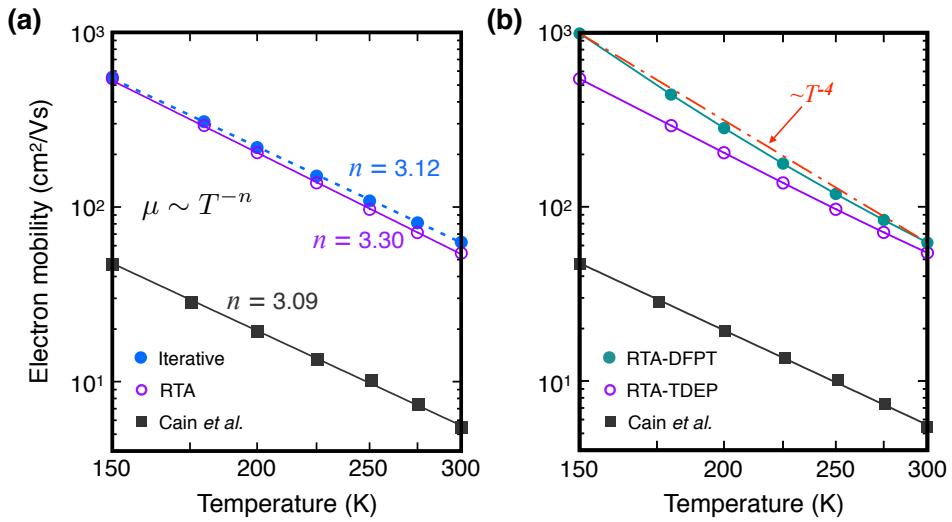

FIG. S2. (a) Electron mobility computed using e-ph matrix elements from the TDEP method. The mobility obtained using the iterative BTE solution (solid blue circles) and the RTA (open purple circles) are compared with experimental values (black squares) taken from Ref. [8]. (b) Electron mobility computed using e-ph matrix elements from the TDEP method (open purple circles) and the DFPT method (solid teal circles), using the RTA in both cases. The red dashed line shows the roughly T^{-4} trend of the DFPT result.

ment with experiment ($T^{-3.09}$) than the RTA result ($T^{-3.30}$). The iterative BTE mobility is roughly 15% higher than the RTA result at room temperature and is close to the RTA result at lower temperature.

Figure S2(b) compares the mobility computed in the RTA using e-ph matrix elements obtained from the TDEP and DFPT methods. DFPT predicts unstable phonons with negative frequencies, for which the e-ph matrix elements are not well defined, and introduces large errors in the low-frequency phonon dispersions, as is shown in Fig. 1 of the main text. For these reasons, we exclude the unstable and low-frequency phonons (with energy of less than 10 meV) in our DFPT mobility calculations. The resulting DFPT mobility shows a much stronger temperature dependence than the TDEP result due to the absence of the ferroelectric soft phonon contribution. As shown in Figure S2(b), the DFPT mobility cannot be fitted properly with a T^{-n} power law, but it exhibits a roughly T^{-4} temperature dependence, versus a $T^{-3.1}$ trend in our TDEP calculations and in experiment.

* bmarco@caltech.edu

[1] X. Gonze, J.-C. Charlier, D. Allan, and M. Teter, Phys. Rev. B **50**, 13035 (1994).

[2] W. Frank, C. Elsässer, and M. Fähnle, Phys. Rev. Lett. **74**, 1791 (1995).

[3] K. Parlinski, Z. Q. Li, and Y. Kawazoe, Phys. Rev. Lett. **78**, 4063 (1997).

[4] P. Giannozzi, S. de Gironcoli, P. Pavone, and S. Baroni, Phys. Rev. B **43**, 7231 (1991).

[5] O. Hellman, I. A. Abrikosov, and S. I. Simak, Phys. Rev. B **84**, 180301 (2011); O. Hellman and I. A. Abrikosov, Phys. Rev. B **88**, 144301 (2013); O. Hellman, P. Steneteg, I. A. Abrikosov, and S. I. Simak, Phys. Rev. B **87**, 104111 (2013).

[6] J. P. Perdew, A. Ruzsinszky, G. I. Csonka, O. A. Vydrov, G. E. Scuseria, L. A. Constantin, X. Zhou, and K. Burke, Phys. Rev. Lett. **100**, 136406 (2008).

[7] A. Janotti, D. Steiauf, and C. G. Van de Walle, Phys. Rev. B **84**, 201304 (2011).

[8] T. A. Cain, A. P. Kajdos, and S. Stemmer, Appl. Phys. Lett. **102**, 182101 (2013).